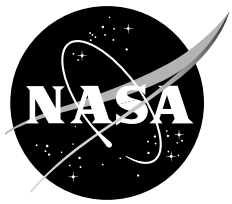
NASA/TM–2008-215358



Fully Automated Single-Zone Elliptic Grid Generation for Mars Science Laboratory (MSL) Aeroshell and Canopy Geometries

Upender K. Kaul
NASA Advanced Supercomputing (NAS) Division
Ames Research Center, Moffett Field, California

July 2008

The NASA STI Program Office . . . in Profile

Since its founding, NASA has been dedicated to the advancement of aeronautics and space science. The NASA Scientific and Technical Information (STI) Program Office plays a key part in helping NASA maintain this important role.

The NASA STI Program Office is operated by Langley Research Center, the Lead Center for NASA's scientific and technical information. The NASA STI Program Office provides access to the NASA STI Database, the largest collection of aeronautical and space science STI in the world. The Program Office is also NASA's institutional mechanism for disseminating the results of its research and development activities. These results are published by NASA in the NASA STI Report Series, which includes the following report types:

- TECHNICAL PUBLICATION. Reports of completed research or a major significant phase of research that present the results of NASA programs and include extensive data or theoretical analysis. Includes compilations of significant scientific and technical data and information deemed to be of continuing reference value. NASA's counterpart of peer-reviewed formal professional papers but has less stringent limitations on manuscript length and extent of graphic presentations.

- TECHNICAL MEMORANDUM. Scientific and technical findings that are preliminary or of specialized interest, e.g., quick release reports, working papers, and bibliographies that contain minimal annotation. Does not contain extensive analysis.

- CONTRACTOR REPORT. Scientific and technical findings by NASA-sponsored contractors and grantees.

- CONFERENCE PUBLICATION. Collected papers from scientific and technical conferences, symposia, seminars, or other meetings sponsored or cosponsored by NASA.

- SPECIAL PUBLICATION. Scientific, technical, or historical information from NASA programs, projects, and missions, often concerned with subjects having substantial public interest.

- TECHNICAL TRANSLATION. English-language translations of foreign scientific and technical material pertinent to NASA's mission.

Specialized services that complement the STI Program Office's diverse offerings include creating custom thesauri, building customized databases, organizing and publishing research results . . . even providing videos.

For more information about the NASA STI Program Office, see the following:

- Access the NASA STI Program Home Page at *http://www.sti.nasa.gov*

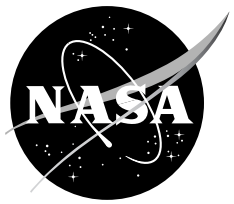
- E-mail your question via the Internet to help@sti.nasa.gov

- Fax your question to the NASA Access Help Desk at (301) 621-0134

- Telephone the NASA Access Help Desk at (301) 621-0390

- Write to:
 NASA Access Help Desk
 NASA Center for AeroSpace Information
 7115 Standard Drive
 Hanover, MD 21076-1320

NASA/TM–2008-215358



Fully Automated Single-Zone Elliptic Grid Generation for Mars Science Laboratory (MSL) Aeroshell and Canopy Geometries

Upender K. Kaul
NASA Advanced Supercomputing (NAS) Division
Ames Research Center, Moffett Field, California

National Aeronautics and
Space Administration

Ames Research Center
Moffett Field, California 94035-1000

July 2008

Acknowledgments

This work was supported by the Supersonics Project of the Fundamental Aeronautics Program. The author gratefully acknowledges the MSL aeroshell and canopy geometry definitions provided by Ed Schairer and Jim Ross.

Available from:

NASA Center for AeroSpace Information
7115 Standard Drive
Hanover, MD 21076-1320
(301) 621-0390

National Technical Information Service
5285 Port Royal Road
Springfield, VA 22161
(703) 487-4650

TABLE OF CONTENTS

ABSTRACT 1
1. INTRODUCTION 1
2. FORMULATION 1
3. RESULTS 5
4. CONCLUDING REMARKS 6
5. REFERENCES 7
6. FIGURES 8

LIST OF FIGURES

Figure 1. Grid over the MSL aeroshell geometry. 8

Figure 2. Cross-section of the elliptic grid around the MSL aeroshell; outer boundary is farfield. 9

Figure 3. Cross-section of the elliptic grid around the MSL aeroshell and the wind-tunnel wall. 10

Figure 4. A 3-D slice of the grid in the vicinity of the aeroshell. 11

Figure 5. Axisymmetric pressure contours about the aeroshell in low speed turbulent flow, $Re = 10^7$. 11

Figure 6. A continuous single-zone grid over the MSL disk-band-gap canopy geometry. 12

Figure 7. Pressure contours over the MSL canopy in low speed laminar flow. 12

FULLY AUTOMATED SINGLE-ZONE ELLIPTIC GRID GENERATION FOR MARS SCIENCE LABORATORY (MSL) AEROSHELL AND CANOPY GEOMETRIES

Upender K. Kaul[1]

Ames Research Center

ABSTRACT

A procedure for generating smooth uniformly clustered single-zone grids using enhanced elliptic grid generation[2,3] has been demonstrated here for the Mars Science Laboratory (MSL) geometries such as aeroshell and canopy, and it has been incorporated in the software. The procedure obviates the need for generating multizone grids for such geometries, as reported in the literature. This has been possible because the enhanced elliptic grid generator automatically generates clustered grids without manual prescription of decay parameters needed with the conventional approach. In fact, these decay parameters are calculated as decay functions as part of the solution, and they are not constant over a given boundary. Since these decay functions vary over a given boundary, orthogonal grids near any arbitrary boundary can be clustered automatically without having to break up the boundaries and the corresponding interior domains into various zones for grid generation.

1. INTRODUCTION

A smooth and orthogonal grid around arbitrary geometries is invariably generated using grid generation techniques based on the solution of partial differential equations. One such powerful technique is based on the solution of elliptic partial differential equations. Elliptic grid generation methods are generally used to create smooth grids on which accurate numerical solutions (ref. 1) to a given physical problem are obtained. This involves the numerical solution of inhomogeneous elliptic partial differential equations. The inclusion of inhomogeneous terms in these equations allows a grid to satisfy clustering and orthogonality properties in the vicinity of specific surfaces in three dimensions, and in the vicinity of specific lines in two dimensions. Elliptic grids yield more accurate predictions, in general, as compared with other grid generation techniques (ref. 1).

2. FORMULATION

Two-dimensional (2-D) form of the inhomogeneous elliptic partial differential equations (PDES) for grid generation was first proposed by Thompson et al. (ref. 2). These 2-D PDES contained four explicit parameters that need to be prescribed by the user. Later, Steger and Sorenson (ref. 3)

[1] NASA Advanced Supercomputing (NAS) Division
[2] U.S. patent 7231329
[3] EEGG3D

prescribed a semi-automatic scheme that reduced the requirement for explicit prescription of these parameters to the two parameters, called decay parameters. In a subsequent study (ref. 4), the author further enhanced this methodology to fully automate the elliptic grid generation process that completely eliminated the need for the explicit user prescription of decay parameters.

Additionally, in the enhanced fully automated methodology (ref. 4), the decay parameters are no longer a specified set of constants chosen manually for the four boundaries for 2-D applications, but four decay functions, each a function of one independent coordinate variable over a given boundary, which are calculated as part of the solution process. This feature makes it possible to cluster a grid normal to any arbitrarily shaped boundary.

Below, a three-dimensional (3-D) analog of the earlier 2-D methodology (ref. 2) is given. Then, the development of the semi-automatic (ref. 3) and the enhanced fully automated (ref. 4) methodologies is briefly discussed. Finally, the extension of the fully automated methodology (ref. 4) for 3-D applications is discussed.

Three-dimensional governing equations for elliptic grid generation are expressed as:

$$\xi_{xx} + \xi_{yy} + \xi_{zz} = P(\xi,\eta,\zeta) = -a_i \cdot \mathrm{sgn}(\xi - \xi_i) \exp\{-b_i|\xi - \xi_i|\}, \quad (1)$$

$$\eta_{xx} + \eta_{yy} + \eta_{zz} = Q(\xi,\eta,\zeta) = -c_i \cdot \mathrm{sgn}(\eta - \eta_i) \exp\{-d_i|\eta - \eta_i|\}, \quad (2)$$

$$\zeta_{xx} + \zeta_{yy} + \zeta_{zz} = R(\xi,\eta,\zeta) = -e_i \cdot \mathrm{sgn}(\zeta - \zeta_i) \exp\{-f_i|\zeta - \zeta_i|\}, \quad (3)$$

where ξ, η and ζ are generalized curvilinear coordinates, x, y and z are Cartesian coordinates, and $P(\xi,\eta,\zeta)$, $Q(\xi,\eta,\zeta)$, and $R(\xi,\eta,\zeta)$, are inhomogeneous terms; a_i, b_i, c_i, d_i, e_i and f_i are manually selected constants, and the subscript "i" refers to a particular boundary component associated with the problem.

A simplified 2-D form of equations (1–3) is written as (ref. 3)

$$\xi_{xx} + \xi_{yy} = -a_i \cdot \mathrm{sgn}(\eta - \eta_i) \exp\{-d_i|\eta - \eta_i|\}, \quad (4)$$

$$\eta_{xx} + \eta_{yy} = -c_i \cdot \mathrm{sgn}(\eta - \eta_i) \exp\{-d_i|\eta - \eta_i|\}, \quad (5)$$

Equations (4) and (5) were used by the authors to semi-automatically generate the 2-D grids with appropriate clustering and orthogonality at the walls. However, the decay parameter, d_i, needed to be set manually, for a given boundary, η_i.

As mentioned previously, the present fully automatic boundary procedure was proposed (ref. 4) to eliminate the need for manual selection of the decay parameters for each boundary. Also, these decay functions, no longer constants, but functions of the independent coordinate variables along a given boundary, were calculated as part of the solution process. This fully automatic boundary procedure has been used successfully for various 2-D complex geometries (ref. 4).

In this paper, extension of the formulation for this automatic procedure for 3-D applications is presented. Geometries chosen here are the geometries for the Mars Science Laboratory (MSL) aeroshell and canopy. The present procedure makes it possible to generate single-zone grids for the aeroshell and canopy geometries.

Using the fully automated approach (ref. 4), for a given boundary, ζ_i ($\zeta > \zeta_i$), for example, equations (1), (2), and (3) are modified here in the context of equations (4) and (5) and are written in the following form.

$$\xi_{xx} + \xi_{yy} + \xi_{zz} = p_3(\xi,\eta,\zeta) \tag{6}$$

where, $p_3(\xi,\eta,\zeta) = -a_{3,i}(\xi,\eta)\ \mathrm{sgn}(\zeta - \zeta_i)\ \exp\{- f_i(\xi,\eta)|\zeta - \zeta_i|\}$

$$\approx (-a_{3,i}(\xi,\eta) + a_{3,i}(\xi,\eta)\ f_i(\xi,\eta)\ (\zeta - \zeta_i))\ \mathrm{sgn}(\zeta - \zeta_i)$$

$$\eta_{xx} + \eta_{yy} + \eta_{zz} = q_3(\xi,\eta,\zeta), \tag{7}$$

where, $q_3(\xi,\eta,\zeta) = -c_{3,i}(\xi,\eta)\ \mathrm{sgn}(\zeta - \zeta_i)\ \exp\{- f_i(\xi,\eta)|\zeta - \zeta_i|\}$

$$\approx (-c_{3,i}(\xi,\eta) + c_{3,i}(\xi,\eta)\ f_i(\xi,\eta)\ (\zeta - \zeta_i))\ \mathrm{sgn}(\zeta - \zeta_i)$$

$$\zeta_{xx} + \zeta_{yy} + \zeta_{zz} = r_3(\xi,\eta,\zeta), \tag{8}$$

where, $r_3(\xi,\eta,\zeta) = -e_{3,i}(\xi,\eta)\ \mathrm{sgn}(\zeta - \zeta_i)\ \exp\{- f_i(\xi,\eta)|\zeta - \zeta_i|\},$

$$\approx (-e_{3,i}(\xi,\eta) + e_{3,i}(\xi,\eta)\ f_i(\xi,\eta)\ (\zeta - \zeta_i))\ \mathrm{sgn}(\zeta - \zeta_i)$$

and, where $a_{k,i} = a_{k,i}(\xi,\eta)$, $c_{k,i} = c_{k,i}(\xi,\eta)$, and $e_{k,i} = e_{k,i}(\xi,\eta)$ and where k = 3 corresponds to the ζ boundary, under consideration.

Similar expressions hold for the inhomogeneous terms for the ξ (k=1) and η (k=2) boundaries.

The positive decay parameters, b_i, d_i and f_i, for the corresponding boundaries, ξ, η and ζ, respectively, are expressed as parameter functions, $b_i(\eta,\zeta)$, $d_i(\xi,\zeta)$, and $f_i(\xi,\eta)$ in the present approach, and the corresponding terms, $a_{2,i}(\xi,\zeta)$, $c_{2,i}(\xi,\zeta)$, $e_{2,i}(\xi,\zeta)$ and $a_{1,i}(\eta,\zeta)$, $c_{1,i}(\eta,\zeta)$, $e_{1,i}(\eta,\zeta)$, hold for η and ξ boundaries respectively.

Without loss of generality, one can consider the neighborhood of a given ζ-boundary segment i, $\zeta - \zeta_i \geq 0$. It can be shown that in a selected region on one side of this boundary segment, where $f_i(\xi,\eta)(\zeta - \zeta_i) << 1$, the governing equations and the inhomogeneous terms have the limiting forms as given in reference 4.

Treatment of a boundary segment, $(\zeta - \zeta_i) < 0$, is analogous. Similar PDES hold for regions close to ξ-boundary and η-boundary segments.

Rewriting, the limiting governing equations near a ζ boundary become (ref. 4)

$$\xi_{xx} + \xi_{yy} + \xi_{zz} - a_{3,i}(\xi,\eta)\, f_i(\xi,\eta)\, (\zeta - \zeta_i) = -a_{3,i}(\xi,\eta)$$
$$\eta_{xx} + \eta_{yy} + \eta_{zz} - c_{3,i}(\xi,\eta)\, f_i(\xi,\eta)\, (\zeta - \zeta_i) = -c_{3,i}(\xi,\eta)$$
$$\zeta_{xx} + \zeta_{yy} + \zeta_{zz} - e_{3,i}(\xi,\eta)\, f_i(\xi,\eta)\, (\zeta - \zeta_i) = -e_{3,i}(\xi,\eta)$$

It can be easily seen that the PDES shown previously represent a self-adjoint operator of the form,

$$L(\theta) = \mathrm{div}(k\, \mathrm{grad}(\theta)) - q\theta$$

and, therefore, boundary constraints, valid in the neighborhood of each of the six boundary segments, are incorporated by applying Green's theorem in three dimensions. For example, for the ζ boundary, the constraint will be given by

$$\int_S (\partial\theta/\partial n)\, d\sigma = \int_V \{-e_{3,i}(\xi,\eta)\, \mathrm{sgn}(\zeta - \zeta_i) + e_{3,i}(\xi,\eta)\, f_i(\xi,\eta)\, \theta\}\, d\tau, \tag{9}$$

where $\theta = (\xi,\eta,\zeta)$, $d\sigma$ is a differential area element, $d\tau$ is a differential volume element, n refers to a direction that is locally normal to a bounding surface S representing a totality of six surfaces including the boundary segments of interest, and V is a volume enclosed by S. This integral-type boundary constraint can be used to calculate the decay parameter analog, $e_{3,i}(\eta,\zeta)f_i(\xi,\eta)$. Similar constraints can be used to calculate the decay parameter analogs, $a_{1,i}(\eta,\zeta)b_i(\eta,\zeta)$, and $c_{2,i}(\eta,\zeta)d_i(\xi,\zeta)$. When expressed in terms of the generalized coordinate, ζ, the boundary constraint given in equation (9) can be written as follows.

$$\int_S I\, d\sigma = \int_S (\partial\theta/\partial n)\, d\sigma = \int_S (\partial\zeta/\partial n)\, d\sigma \tag{10}$$

The integral $\int_S I\, d\sigma$ in equation (10) can be written as an algebraic sum of six integrals, evaluated over the indicated boundary segments:

$$\int_S I\, d\sigma = \int_{\xi max} I\, d\sigma + \int_{\eta max} I\, d\sigma + \int_{\zeta max} I\, d\sigma - \int_{\xi min} I\, d\sigma - \int_{\eta min} I\, d\sigma - \int_{\zeta min} I\, d\sigma \tag{11}$$

where the surface configurations ξmax, ξmin, etc. represent the corresponding boundary segments that together make up the surface S. For the first and fourth integral pair, the second and fifth integral pair, and the third and sixth integral pair in equation (11), the following respective relations are derived.

$$\int_\xi I\, d\sigma = \int_\xi (1/J\sqrt{\alpha_{11}})\, \alpha_{13}\, [(x_\eta^2 + y_\eta^2 + z_\eta^2)\, (x_\zeta^2 + y_\zeta^2 + z_\zeta^2)]^{1/2}\, d\zeta\, d\eta. \tag{12}$$
$$\int_\eta I\, d\sigma = \int_\eta (1/J\sqrt{\alpha_{22}})\, \alpha_{23}\, [(x_\xi^2 + y_\xi^2 + z_\eta^2)\, (x_\zeta^2 + y_\zeta^2 + z_\zeta^2)]^{1/2}\, d\xi\, d\zeta, \tag{13}$$
$$\int_\zeta I\, d\sigma = \int_\zeta (1/J)\, [\alpha_{33}\, (x_\eta^2 + y_\eta^2 + z_\eta^2)\, (x_\xi^2 + y_\xi^2 + z_\xi^2)]^{1/2}\, d\eta\, d\xi, \tag{14}$$

$$\alpha_{11} = J^2(\xi_x^2 + \xi_y^2 + \xi_z^2),$$
$$\alpha_{22} = J^2(\eta_x^2 + \eta_y^2 + \eta_z^2),$$
$$\alpha_{33} = J^2(\zeta_x^2 + \zeta_y^2 + \zeta_z^2),$$

$$\alpha_{12} = J^2(\xi_x\eta_x + \xi_y\eta_y + \xi_z\eta_z),$$
$$\alpha_{13} = J^2(\xi_x\zeta_x + \xi_y\zeta_y + \xi_z\zeta_z),$$
$$\alpha_{23} = J^2(\eta_x\zeta_x + \eta_y\zeta_y + \eta_z\zeta_z),$$

where $J = J((x,y,z)/(\xi,\eta,\zeta))$ is a Jacobian of the transformation (x,y,z) --> (ξ,η,ζ).

Equations (12)–(14) can be used to express the boundary constraints in the computational space (generalized variables). The following governing equations in computational space are solved, subject to the boundary constraints derived above.

$$\alpha_{11}\, x_{i,\xi\xi} + \alpha_{22}\, x_{i,\eta\eta} + \alpha_{33}\, x_{i,\zeta\zeta} + 2\{\alpha_{12}\, x_{i,\xi\eta} + \alpha_{13}\, x_{i,\xi\zeta} + \alpha_{23}\, x_{i,\eta\zeta}) =$$
$$-J^2\{\, p_3\, x_{i,\xi} + q_3\, x_{i,\eta} + r_3\, x_{i,\zeta}\,\},$$
x_i = x, y or z.

A decay parameter analog, such as $e_{3,i}(\xi,\eta)f_i(\xi,\eta)$, may vary with one or more of the generalized coordinates, such as (ξ,η), rather than being constant; and this variation is determined as part of the solution of the grid problem, rather than being prescribed initially by the user. This grid solution can be determined for either a static grid or a dynamically changing grid. Hence, dynamically changing grids can be generated automatically without the user intervention.

The preceding analysis has focused on the neighborhoods of the grid boundary segments. As noted in the preceding, in an interior region, far from the grid boundary segments, the defining partial differential equations become homogeneous, and an orthogonal and uniform grid cell distribution is obtained which smoothly transitions from the interior to the boundaries.

3. RESULTS

Some key elements of enhanced elliptic grid generation methodology are demonstrated through a few selected computational grid generation examples. The geometries for planetary entry descent and landing systems, such as an aeroshell and a canopy for the Mars Science Laboratory (MSL), are considered here. Single-zone grids are generated with the present grid generation procedure which are uniformly clustered at the body. With the conventional elliptic grid generation methodology, decay parameters are prescribed by the user as constants over a boundary. If the boundary slope is discontinuous, then this prescription fails to generate uniformly clustered grids around sharp corners and high curvature regions. To avoid this problem in the conventional approach, grids are typically decomposed into multiple zones and the grids are generated separately for these zones.

In the present methodology, decay parameters are automatically calculated as decay functions, as part of the solution. Thus, a uniformly clustered grid is generated over an arbitrarily shaped boundary as a single zone grid. The grid over the MSL aeroshell geometry, shown in figure 1, is generated as a single-zone 51x72x61 grid; 72 points in the meridional direction, 51 points in the streamwise direction, and 61 points in the direction normal to the body. An axisymmetric cross-section, 51x61, of the volume grid around the aeroshell is shown in figure 2. This grid is shown to be clustered at the

aeroshell wall. Away from the aeroshell, the grid uniformly stretches to the farfield boundary. No clustering requirement is enforced at the farfield boundary. As shown, the grid generated is orthogonal and uniformly clustered at the aeroshell surface.

Figure 3 shows the elliptic grid around the aeroshell bounded by a tunnel wall. Therefore, the grid is clustered at both the aeroshell and tunnel walls showing uniform clustering at the tunnel wall corner points. Conventional methods fail to enforce clustering in the neighborhood of these discontinuities. A 3-D slice through the volume grid including the aeroshell surface is shown in figure 4.

One of the key elements of the enhanced elliptic grid generation procedure is that since the decay function varies over the body surface, it can automatically resolve the curvature of the surface in accordance with the clustering requirement. It is clearly not possible to prescribe such a decay function manually that is required with the conventional elliptic grid generation schemes.

As an example, a low speed turbulent flow calculation at a Reynolds number of $2x10^7$ was carried out with the k-ε turbulence model (refs. 5, 6), and the corresponding pressure contours over the aeroshell are shown in figure 5. The flow solver (ref. 7) used for this calculation is a low speed flow solver.

Another grid calculation was carried out for the MSL disk-band-gap canopy, and the grid over the canopy geometry is shown in figure 6. Again, the grid shown in figure 5 represents a single-zone grid. Pressure contours over the canopy in low speed laminar flow are shown in figure 7.

4. CONCLUDING REMARKS

A fully automated 3-D elliptic grid generation method has been developed and demonstrated for the 3-D MSL geometries such as the aeroshell and canopy. Clustered body-orthogonal grids for the MSL aeroshell and the canopy were generated automatically without any user intervention to enforce the clustering properties. This makes the 3-D enhanced elliptic grid generator a powerful tool for generation of the volume grids around complex geometries, especially the deforming grids about the deploying geometries such as MSL canopies and the inflatable aerodynamic decelerators.

5. REFERENCES

1. Kaul, U. K. and Chaussee, D. S.: A Comparative Study of the Parabolized Navier-Stokes (PNS) Code Using Various Grid Generation Techniques. Int. J. Computers & Fluids, vol. 13, no. 4, 1985, pp. 421-441.

2. Thompson, J. F.; Thames, F. C.; and Mastin, C. W.: TOMCAT – A Code for Numerical Generation of Boundary-Fitted Curvilinear Coordinate Systems on Fields Containing Any Number of Arbitrary Two-Dimensional Bodies. J. Computational Physics, vol. 24, 1977, pp. 274-302.

3. Steger, J. L. and Sorenson, R. L.: Automatic Mesh-Point Clustering Near a Boundary in Grid Generation with Elliptic Partial Differential Equations. J. Comp. Physics, vol. 33, 1979, pp. 405-410.

4. Kaul, U. K.: New Boundary Constraints for Elliptic Systems Used in Grid Generation Problems. J. Comp. Physics, vol. 189, 2003, pp. 476-492.

5. Kaul, U. K.: An Implicit Finite Difference Code for a Two-Equation Turbulence Model for 3-D Flows. NASA TM-85241, June 1985.

6. Kaul, U. K.: A Fully Implicit Numerical Scheme for the Solution of Transport Equations in Fluid Dynamics. Numerical Methods in Laminar and Turbulent Flow, eds. C. Taylor, J. H. Chin and G. M. Homsy, vol. 2, 1991, Pineridge Press, Swansea, U. K., pp. 1724-1733.

7. Kaul, U. K. and Shreeve, R. P.: A Fully Viscous Navier-Stokes Formulation in Generalized Curvilinear Coordinates for Prediction of Internal Turbine Blade-Cooling Flows. AIAA J. of Thermophysics and Heat Transfer, vol. 10, no. 4, Oct.-Dec., 1996.

6. FIGURES

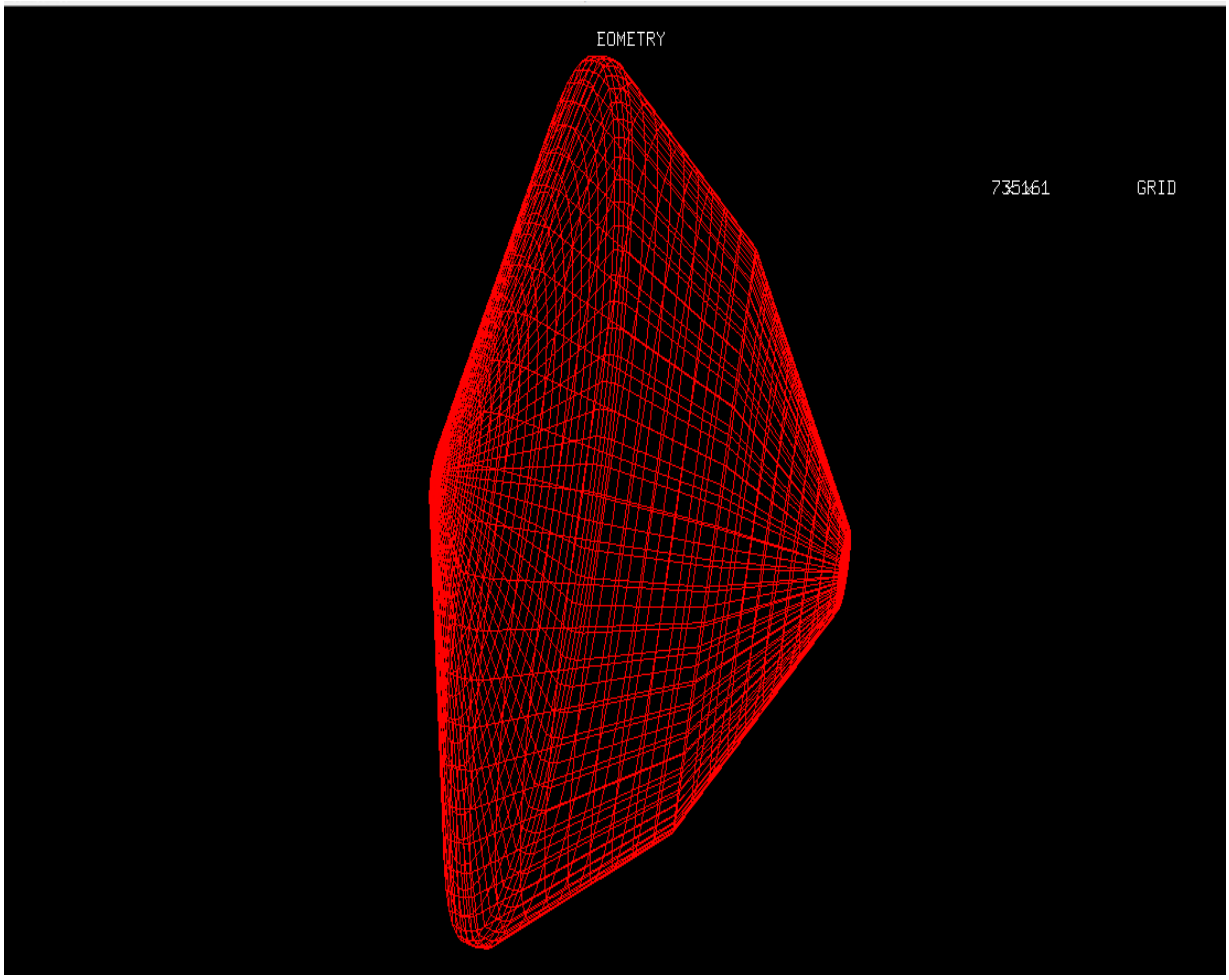
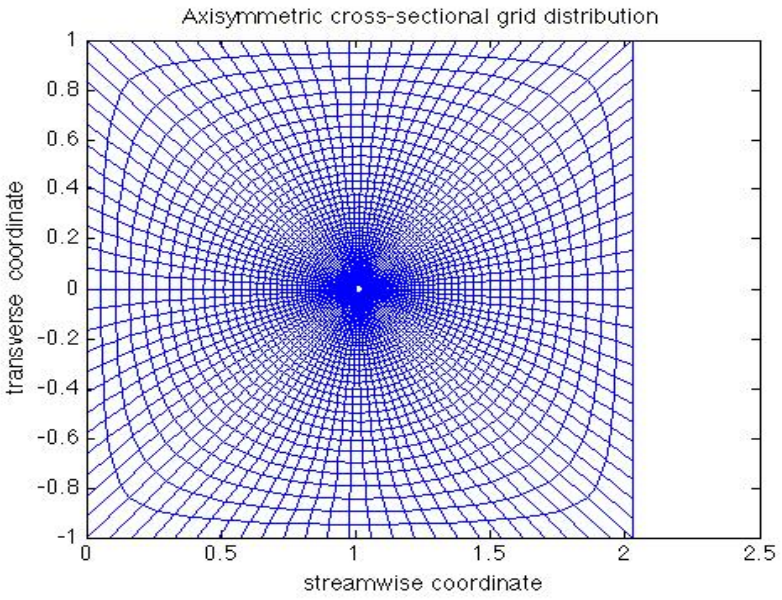
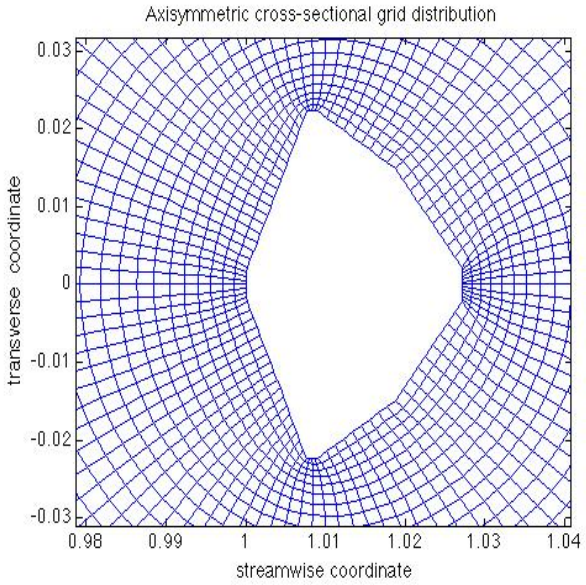


Figure 1. Grid over the MSL aeroshell geometry.

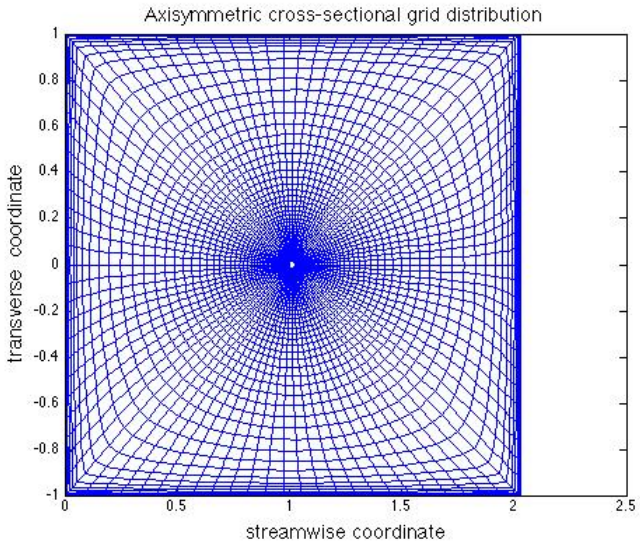


a) Clustering around the aeroshell wall

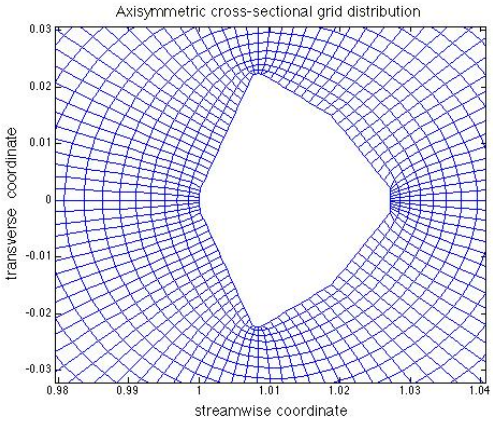


b) Enlarged close to the aeroshell

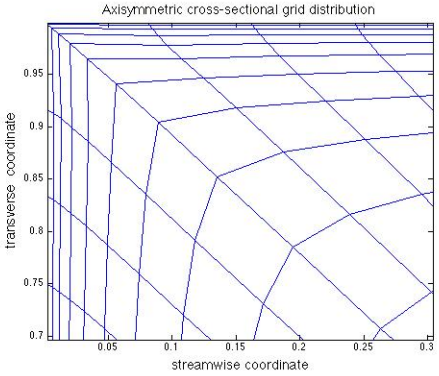
Figure 2. Cross-section of the elliptic grid around the MSL aeroshell; outer boundary is farfield.



a) Clustering around the aeroshell and the wind-tunnel wall



b) Enlarged close to the aeroshell



c) Enlarged close to the tunnel wall

Figure 3. Cross-section of the elliptic grid around the MSL aeroshell and the wind-tunnel wall.

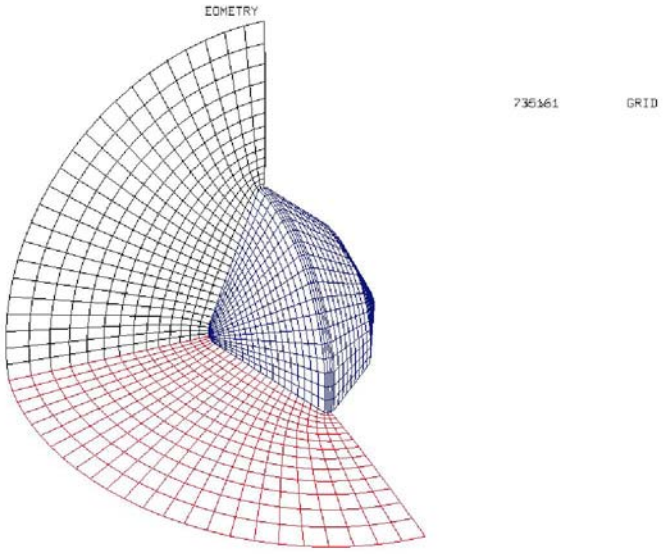


Figure 4. A 3-D slice of the grid in the vicinity of the aeroshell.

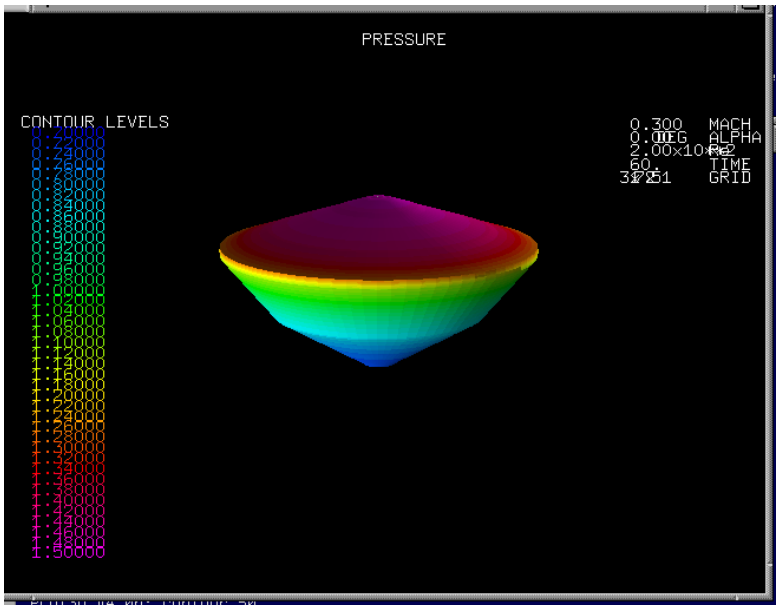


Figure 5. Axisymmetric pressure contours about the aeroshell in low speed turbulent flow, Re = 10^7.

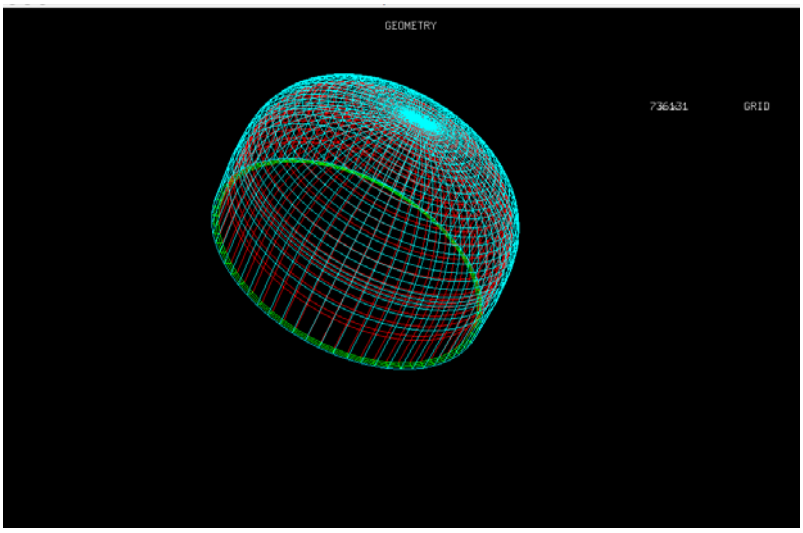


Figure 6. A continuous single-zone grid over the MSL disk-band-gap canopy geometry.

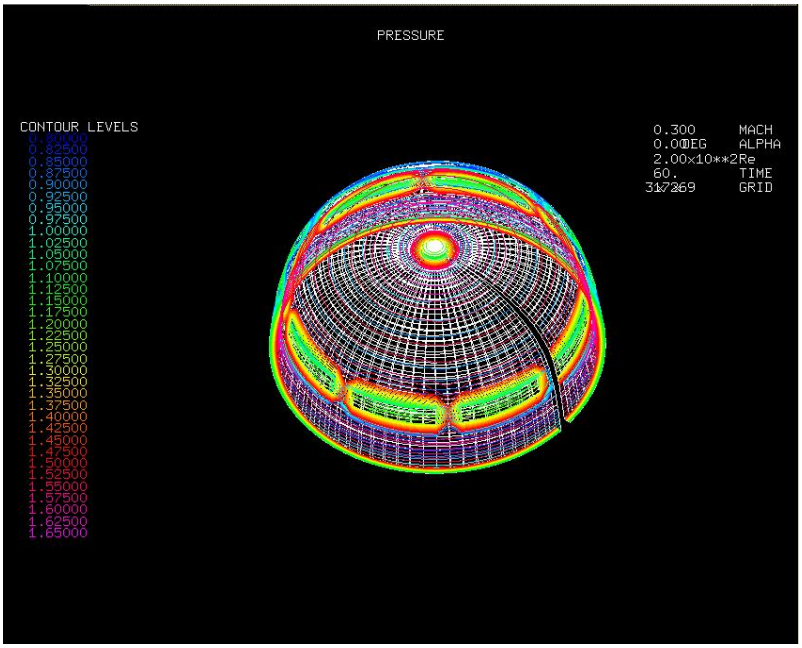


Figure 7. Pressure contours over the MSL canopy in low speed laminar flow.

REPORT DOCUMENTATION PAGE

Form Approved
OMB No. 0704-0188

The public reporting burden for this collection of information is estimated to average 1 hour per response, including the time for reviewing instructions, searching existing data sources, gathering and maintaining the data needed, and completing and reviewing the collection of information. Send comments regarding this burden estimate or any other aspect of this collection of information, including suggestions for reducing this burden, to Department of Defense, Washington Headquarters Services, Directorate for information Operations and Reports (0704-0188), 1215 Jefferson Davis Highway, Suite 1204, Arlington, VA 22202-4302. Respondents should be aware that notwithstanding any other provision of law, no person shall be subject to any penalty for failing to comply with a collection of information if it does not display a currently valid OMB control number.
PLEASE DO NOT RETURN YOUR FORM TO THE ABOVE ADDRESS.

1. REPORT DATE *(DD-MM-YYYY)*	2. REPORT TYPE	3. DATES COVERED *(From - To)*
07/07/2008	Technical Memorandum	

4. TITLE AND SUBTITLE
Fully Automated Single-Zone Elliptic Grid Generation for Mars Science Laboratory (MSL) Aeroshell and Canopy Geometries

5a. CONTRACT NUMBER

5b. GRANT NUMBER

5c. PROGRAM ELEMENT NUMBER

6. AUTHOR(S)
Upender K. Kaul

5d. PROJECT NUMBER

5e. TASK NUMBER

5f. WORK UNIT NUMBER
WBS 984754.02.07.01.22.04

7. PERFORMING ORGANIZATION NAME(S) AND ADDRESS(ES)
National Advanced Supercomputing (NAS) Division
Ames Research Center, Moffett Field, CA 94035-1000

8. PERFORMING ORGANIZATION REPORT NUMBER
A-080009

9. SPONSORING/MONITORING AGENCY NAME(S) AND ADDRESS(ES)
National Aeronautics and Space Administration
Washington, D. C. 20546-0001

10. SPONSORING/MONITOR'S ACRONYM(S)
NASA

11. SPONSORING/MONITORING REPORT NUMBER
NASA/TM–2008-215358

12. DISTRIBUTION/AVAILABILITY STATEMENT
Unclassified—Unlimited Distribution: Nonstandard
Subject Category: 01, 34, 39, 59, 61
Availability: NASA CASI (301) 621-0390

13. SUPPLEMENTARY NOTES
Point of Contact: Upender K. Kaul, Ames Research Center, MS 258-5, Moffett Field, CA 94035-1000
(650) 604-2973

14. ABSTRACT
A procedure for generating smooth uniformly clustered single-zone grids using enhanced elliptic grid generation has been demonstrated here for the Mars Science Laboratory (MSL) geometries such as aeroshell and canopy. The procedure obviates the need for generating multizone grids for such geometries, as reported in the literature. This has been possible because the enhanced elliptic grid generator automatically generates clustered grids without manual prescription of decay parameters needed with the conventional approach. In fact, these decay parameters are calculated as decay functions as part of the solution, and they are not constant over a given boundary. Since these decay functions vary over a given boundary, orthogonal grids near any arbitrary boundary can be clustered automatically without having to break up the boundaries and the corresponding interior domains into various zones for grid generation.

15. SUBJECT TERMS
Enhanced elliptic grid generation, decay functions, grid clustering, single-zone grids, Mars Science Laboratory (MSL), canopy and aeroshell grids, inflatable aerodynamic decelerator (IAD)

16. SECURITY CLASSIFICATION OF:			17. LIMITATION OF ABSTRACT	18. NUMBER OF PAGES	19a. NAME OF RESPONSIBLE PERSON
a. REPORT	b. ABSTRACT	c. THIS PAGE			Upender K. Kaul
Unclassified	Unclassified	Unclassified	Unclassified	18	19b. TELEPHONE *(Include area code)* (650) 604-2973